OPTOELECTRONIC DESIGN OF MULTIJUNCTION WIRE-ARRAY SOLAR CELLS

Daniel B. Turner-Evans[1], Michael D. Kelzenberg[1], Chris T. Chen[1],
Emily C. Warmann[1], Adele C. Tamboli[1], and Harry A. Atwater[1,2]
[1]Thomas J. Watson Laboratories of Applied Physics, California Institute of Technology, Pasadena, CA, USA
[2]Kavli Nanoscience Institute, California Institute of Technology, Pasadena, CA, USA

ABSTRACT

Microwire solar cells have demonstrated promising optical and photovoltaic performance in arrays of single junction Si wires. Seeking higher efficiencies, we have numerically investigated III-V on $Si_{1-x}Ge_x$ architectures as candidates for tandem microwire photovoltaics via optical and electronic transport modeling. Optical modeling indicates that light trapping is an important design criterion. Absorption is more than doubled by the presence of Al_2O_3 scattering particles around the wires, leading to high overall light collection despite low wire packing fraction. Texturing of the microwire outer surface, which was found to occur experimentally for GaP/Si microwires, is also shown to enhance absorption by over 50% relative to wires with smooth surfaces, allowing for the use of thinner layers. Finally, full optoelectronic simulations of GaAs on Ge structures revealed that current matching is attainable in these structures and that wire device efficiencies can approach those of planar cells.

INTRODUCTION

Si microwire array solar cells, grown from relatively inexpensive precursors, have demonstrated promising optical and electronic performance. They have been shown to absorb up to 85% of incident sunlight despite using just 1% of the material in an equivalent, planar, wafer-based Si cell [1]. Additionally, effective diffusion lengths in excess of 30 μm have been reported in Si microwires, suggesting that high material quality and effective surface passivation are possible [2]. Arrays grown on templated Si wafers can be embedded in a flexible polymer and peeled from the growth substrate, allowing for Si wafer reuse in a microwire cell fabrication process. Finally, single wire devices have exhibited open circuit voltages (V_{OC}s) of ~600 mV and the potential for greater than 17% efficiencies [2] while large area cells have reached efficiencies of greater than 8%, with many remaining opportunities for design and process improvement [3].

Si microwire arrays have revealed the potential of the wire array architecture, and thus the wire geometry can now be reasonably extended to high efficiency, multijunction devices. $Si_{1-x}Ge_x$ wire array structures, grown by chemical vapor deposition with the vapor-liquid-solid method, can be conformally coated with compound semiconductor layers by metallorganic chemical vapor deposition (MOCVD) to create these high efficiency arrays.[4] While planar, tandem III-V on $Si_{1-x}Ge_x$ cells are limited by large defects densities that result from polar on non-polar growth and lattice mismatch, the unique geometry of the wire structure may be able to mitigate these defects and allow for higher performance cells. Furthermore, the structure may allow for thinner absorber layers, and thus less material, to be used, lowering the overall cost.

Multijunction device designs must optimize light absorption and transport in each subcell to enable current matching between absorber layers. Without quantitative optical full field and electronic finite element models, it is difficult to assess the absorption and transport properties of such photovoltaic structures due to their unconventional device geometry. Here, through simulation, we explore the potential for multijunction microwire photovoltaics, following a similar methodology as has been used previously for wire cells [5, 6].

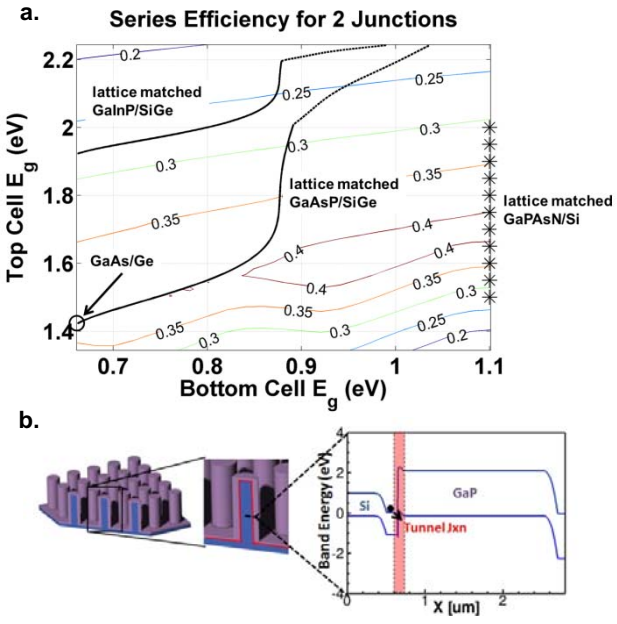

Fig 1. a. Detailed balance efficiency contour plot as a function of top and bottom cell bandgaps. Lattice matched material combinations are noted and suggest desirable material systems for multijunction wire cells. Data is taken from [7, 8] b. A GaP on Si wire array cell, an example of a tandem wire structure comprised of two cells joined by a tunnel junction.

SIMULATION SETUP

Optical models of the wire devices were generating using Lumerical, a finite difference time domain (FDTD) full field electromagnetic simulation tool. Ray-tracing was also investigated, but was unable to capture the full optical effects inherent to structures whose dimensions are on the order of the wavelength. For the FDTD simulations, the bottom boundary was defined to be a perfect reflector, while the top surface of the simulation region, separated 2 μm from the wire, was defined as a perfectly matched layer, implying that reflected light escaping the front is lost. Periodic boundary conditions were employed in the vertical planes to capture wire to wire mode coupling due to the array structure. The wires were arrayed in a square pattern with 7 μm center to center spacing. All excitation was from plane wave sources. The particular wire geometry was varied on a case by case basis.

Device physics models were carried out using Sentaurus, a commercial finite element method device physics simulator. Shockley-Reed-Hall, Auger, and radiative recombination were assumed as well as bandgap narrowing due to high doping, doping dependent mobility, and a tunneling model that included both band to band and two band transitions to account for transport across the tunnel junction. Base doping was set to 5 x 10^{16} cm^{-3} (p-type), emitter doping was set to 9 x 10^{17} cm^{-3} (n-type), and the tunnel region, set to be 40 nm thick, was doped at 5 x 10^{19} cm^{-3} for each type.

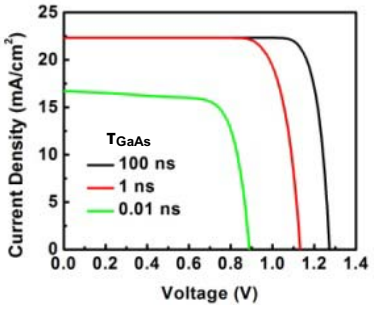

Fig 2. Simulated light IV curves of a planar GaAs/Ge cell for a variety of GaAs lifetimes.

Planar cells were investigated to verify the integrity of the simulations. Fig. 2 shows the light IV curves from a typical planar test structure, consisting of a 500 nm thick GaAs cell on a 10 μm thick Ge cell with a 40 nm thick, highly doped GaAs/Ge tunnel junction connecting the two. The GaAs lifetime is varied, initially reducing the V_{OC} alone, then also affecting the short circuit current (J_{SC}) when the diffusion length becomes on the order of the layer thickness. A recombination velocity of 100 cm/sec is set at the GaAs/Ge tunnel junction interface and at the surfaces. The best performing tandem structure has a J_{SC} of 22.33 mA/cm^2, a V_{OC} of 1.27 V, and an overall efficiency (η) of 24.3%. The GaAs subcell was found to have stand alone J_{SC}, V_{OC}, and η values of 23.6 mA/cm^2, 0.98 V, and 20.22%, respectively, while the Ge cell had corresponding values of 22.36 mA/cm^2, 0.29V, and 4.69%.

DEVICE STRUCTURE

Ge and Si microwires have both been successfully fabricated by the vapor-liquid-solid wire growth process [9, 10] and therefore $Si_{1-x}Ge_x$ can reasonably be assigned as the core material for multijunction wire designs. A variety of materials were considered for the outer shell material, with the constraint that the semiconductor be lattice matched to the underlying $Si_{1-x}Ge_x$ core, as shown in Fig.1a. In particular, we focused on high efficiency $GaN_xP_{1-x-y}As_y$ on Si and $GaAs_xP_{1-x}$ on $Si_{1-x}Ge_x$ combinations.

For an appropriate choice of x and y, MOCVD grown $GaN_xP_{1-x-y}As_y$ can be lattice-matched to Si and will have a suitable bandgap for attaining a high efficiency, tandem structure [11]. Though experimentally-grown $GaN_xP_{1-x-y}As_y$ has, to date, exhibited very short diffusion lengths [11], the wire geometry, which decouples the direction of absorption and carrier collection, may allow for reasonable device performance despite low material quality [12]. A typical $GaN_xP_{1-x-y}As_y$/Si structure is shown in Fig. 1b, where a tunnel junction connects an outer GaP cell to the underlying Si core.

As another option, high quality $GaAs_xP_{1-x}$ can be grown through MOCVD and is widely used in the LED industry. Though the maximum theoretical efficiency for $GaAs_xP_{1-x}$ on $Si_{1-x}Ge_x$ is less than that of $GaN_xP_{1-x-y}As_y$ on Si, high quality films of the material have been successfully grown whereas $GaN_xP_{1-x-y}As_y$ films have yet to demonstrate good electrical quality.

MAXIMIZING ABSORPTION

As shown in [1], Si wire arrays embedded in PDMS with Al_2O_3 scattering particles, a SiN_x ARC, and a back reflector can absorb up to 85% of incident sunlight. Thus, to extend these experimental results to our modeling, simulated GaAs/Ge microwires of varying length were surrounded by Al_2O_3 scattering particles, and the particle density and distribution were systematically varied in order to maximize absorption. Fig. 3a shows an example of the structures investigated. The number of particles per wire was varied as was their distribution. Simulations were run at 500 nm and 1000 nm, and the particle size was restricted to between 50 and 250 nm. Particles were randomly distributed within the stated constraints.

Wire absorption was found to increase with wire length. Additionally, for shorter wires, more scattering particles led to higher absorption at 1000 nm but lower overall absorption at 500 nm. When the number of scattering particles is increased, the 500 nm light can no longer penetrate to the bottom of the array and thus much of it is

reflected without being absorbed. The 1000 nm light, on the other hand, penetrates all the way to the bottom regardless of particle number and is more effectively scattered by a greater number of particles. Thus, a linearly graded distribution of scattering particles was chosen to allow the 500 nm light to reach the bottom of the array, being absorbed by the wire throughout.

Ultimately, after a series of iterations, a 48 μm long wire with 1600 particles per wire arranged in a linearly graded distribution was found to absorb over 55% of both 500 nm and 1000 nm light, more than double the amount of light absorbed for the base case, a 12 μm wire with a back reflector alone. No antireflection coating was employed in these simulations; incorporation one is expected to significantly improve the overall absorption. The magnitude of the electric field for both structures can be seen in Fig. 3b. for 1000 nm and in Fig. 3c. for 500 nm. Simulations of longer wire lengths, which we expect to lead to the experimentally-observed 85% absorption, proved too computationally expensive using FDTD simulations.

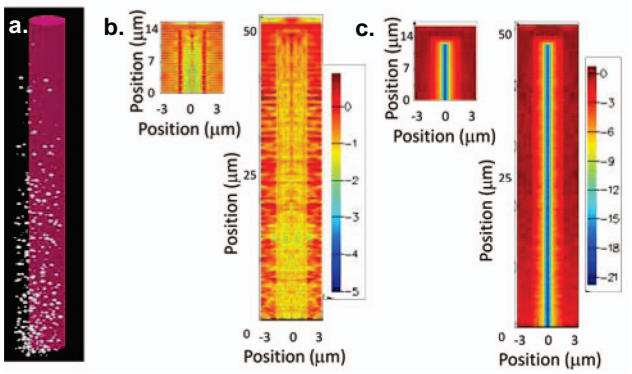

Fig 3. a. A GaAs/Ge wire surrounded by Al_2O_3 scattering particles. b. Log of the electric field magnitude for a 12 μm, stand alone wire and for a 48 μm wire with scattering particles for 1000 nm light. c. Log of the electric field magnitude for the same structures for 500 nm light. The longer wire with scatterers absorbs over 55% of light at both wavelengths, more than double that of the 12 μm long wire.

THE EFFECTS OF SURFACE MORPHOLOGY

The surface morphology of microwires also affects the optical absorption. We have observed that experimentally synthesized conformal GaP/Si wire arrays, which are similar to the GaNPAs structure studied here [4], had a rough surface morphology, as seen in Fig. 4a. Thus, FDTD simulations were performed in order to assess the impact of such rough surfaces on the optical absorption profile. The simulation structure can be seen in Fig. 4b., while the log of the absorbed power for a conformal and a textured wire structure at 500 nm can be seen in Fig. 4c. At this wavelength, in the textured structure, the GaP layer absorbs 33% of the incident power while the Si layer absorbs 45% of the power. In contrast, for the smooth structure, which has more GaP material, the GaP only absorbs only 21% of the power while the Si absorbs 49% of the power. Full field simulations reveal that in the smooth structure, incident light is channeled into waveguide modes in the higher index Si core whereas microwires with rough surface morphology increase the optical path length in the GaP shell and enhance shell absorption. Thus, in order to achieve current matching without using a thick shell material, texturing will be beneficial.

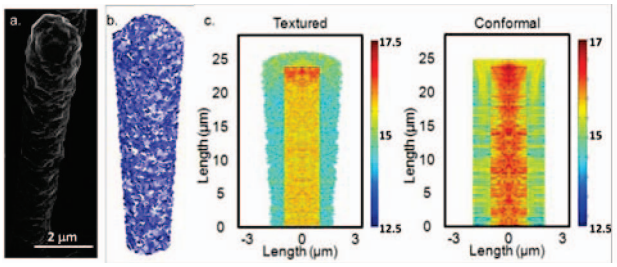

Fig 4. a. SEM image of a GaP on Si wire. b. The simulation geometry of the textured cell. c. The absorbed power, plotted on a log scale, in textured and conformal GaP on Si wires for 500 nm light. Though the textured cell has less GaP, it absorbs more light.

FULL OPTOELECTRONIC DEVICE SIMULATIONS

After exploring the tandem wire array structures' optical properties, a full tandem wire device was created to gain insight into the electronic properties. The chosen architecture consisted of a GaAs shell of varying thickness on a Ge wire core. While GaAs and Ge will not lead to the highest tandem efficiency, as seen in Fig. 1, their materials properties are well known, and the lessons learned from the combination in the wire structures should readily extend to other materials systems. The overall structure consisted of a 0.75 μm radius, 40 μm long Ge wire surrounded by varying conformal thicknesses of GaAs. Scattering particles were employed to boost absorption, as explained above.

Optical generation profiles were created using 2D FDTD simulations. 2D simulations were found to obey the same general trends as the previous 3D simulations and, due to their drastically reduced run time, were necessary in order to achieve a large number of iterations for a variety of GaAs thicknesses and at wavelengths that spanned the AM 1.5G solar spectrum above the bandgap of Ge (0.67 eV). 400 to 1800 nm light was used with steps of 100 nm. The individual wavelengths were then weighted by the binned solar spectrum and summed to create a generation profile that was representative of full solar spectrum excitation.

The first hurdle in achieving a high efficiency tandem structure is current matching between the layers; the J_{SC}

will be limited by the lowest current subcell. Thus, the GaAs shell thickness was varied until the overall core and shell carrier generation were equivalent. Though the simulations were run in 2D, the generation was integrated in cylindrical coordinates to take full account of the volume. Fig. 5 shows the generation profile of three representative wire structures. Waveguide modes were observed to travel down into the base for both the shell and the Ge core. The highest generation rates were at the top of the wires, where the light is incident at full intensity, but appreciable generation also occurred along the length of the wires due to optical redirection of the normally incident waves by the scattering particles. The 250 nm thick shell structure was found to lead to equal overall carrier generation in both materials; though the shell is relatively thin, the direct gap of GaAs is highly absorbing, allowing for a thin film to capture most of the above gap spectrum. Additionally, the cylindrical geometry allows for a relatively high volume of GaAs despite the small radial dimensions.

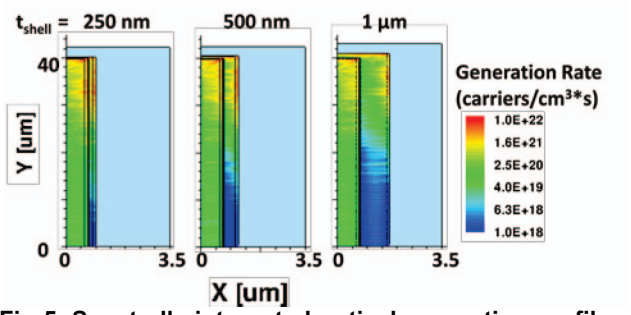

Fig 5. Spectrally integrated optical generation profiles for GaAs on Ge microwires for a variety of GaAs shell thicknesses. The lines delineate the base, emitter, and tunnel junctions of the two materials. Though not visible, scatterers were used in the simulations. The light blue background outlines the overall simulation geometry. The carrier generation is matched for the Ge and GaAs subcells in the 250 nm thick structure.

The generation profiles obtained from the FDTD simulations were then introduced into a device physics model using the parameters of the planar GaAs on Ge cells. Cylindrical symmetry was specified, allowing for quasi-3D simulations. IV curves for the current matched, 250 nm thick GaAs geometry are shown in Fig. 6a. for GaAs material with lifetimes of 100 ns, 1 ns, and 10 ps. They follow the same trends as the planar GaAs cell; a decrease in lifetime leads to a loss in V_{OC} in all cases and a loss in J_{SC} when the diffusion length drops to a value on the order of the film dimensions, limiting overall carrier collection.

Fig. 6b. compares the performance of three cells with 1 ns GaAs lifetimes but differing shell thickness. The thicker GaAs films lead to a loss of photocurrent from the Ge core and hence current matching no longer holds and the J_{SC} drops significantly.

The champion, 250 nm, 100 ns GaAs on Ge wire yielded a V_{OC} of 1.16 V, a J_{SC} of 20.46 mA/cm^2, and a η of 19.74%. While these values are not as high as those found for the planar cell, they are comparable and suggest the full feasibility of creating wire array tandem cells. Improved light trapping and the incorporation of window layers as well as the use of more optimal bandgap combinations could lead to further improvements in device performance. Thus, the tandem wire array structure should be able to achieve efficiencies comparable to planar analogs. The combination of high device quality, low material use, and the ability to embed wire arrays in plastic and peel them off, allowing for both a flexible cell and wafer reuse, makes the tandem wire array architecture worthy area of further investigation.

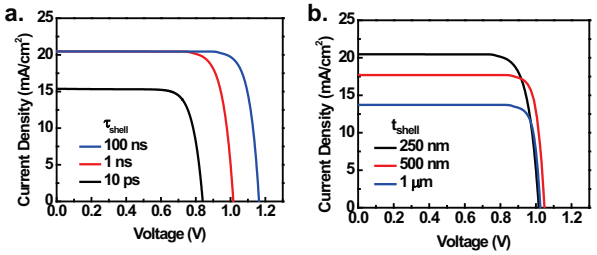

Fig 6 a. Simulated light IV curves of a 250 nm GaAs shell/Ge wire core structure for a variety of shell lifetimes. b. Simulated light IV curves for a variety of GaAs shell thicknesses showing the important of current matching. The lifetime is fixed at 1 ns.

CONCLUSION

We have considered a number of important considerations for the design of multijunction, microwire photovoltaic structures. $GaN_xP_{1-x-y}As_y$ on Si and $GaAs_xP_{1-x}$ on $Si_{1-x}Ge_x$ combinations are predicted to have relatively high efficiencies from simple detailed balance considerations and should benefit from the lowered cost, the flexibility, and the strain management inherent to wire array structures. Scattering particles incorporated into arrays of long microwires allow for higher overall absorption, and texturing of the wire surface, which can be achieved in the growth process, will aid in achieving current matching between conformally-grown subcells. Finally, full optoelectronic simulations of a GaAs on Ge structure reveal the potential of the wire array structure and the ability to current match, demonstrating efficiencies comparable to planar devices despite using far less material.

ACKNOWLEDGMENTS

The author would like to thank Michael G. Deceglie and Nick Strandwitz for useful discussion. Support for this work was provided by DARPA (D.B.T-E., A.T.) and the Department of Energy Basic Energy Sciences, Office of Science through the Light Material Interactions Energy

Frontier Research Center under contract number DE-SC0001293 (MDK and HAA). D.B.T-E. acknowledges the NSF for fellowship support.

REFERENCES

[1] M. D. Kelzenberg*, et al.*, "Enhanced absorption and carrier collection in Si wire arrays for photovoltaic applications," *Nature Materials,* vol. 9, pp. 239-244, Mar 2010.

[2] M. D. Kelzenberg*, et al.*, "High-performance Si microwire photovoltaics," *Energy & Environmental Science,* 2011.

[3] M. C. Putnam*, et al.*, "Si microwire-array solar cells," *Energy & Environmental Science,* vol. 3, pp. 1037-1041, 2010.

[4] A. C. Tamboli*, et al.*, "Conformal GaP layers on Si wire arrays for solar energy applications," *Applied Physics Letters,* vol. 97, pp. 221914-3, 2010.

[5] M. D. Kelzenberg*, et al.*, "Predicted efficiency of Si wire array solar cells," in *Photovoltaic Specialists Conference (PVSC), 2009 34th IEEE*, 2009, pp. 001948-001953.

[6] E. Pickett*, et al.*, "Faceting and disorder in nanowire solar cell arrays," in *Photovoltaic Specialists Conference (PVSC), 2010 35th IEEE*, 2010, pp. 001848-001853.

[7] R. Braunstein*, et al.*, "Intrinsic Optical Absorption in Germanium-Silicon Alloys," *Physical Review,* vol. 109, p. 695, 1958.

[8] I. Vurgaftman*, et al.*, "Band parameters for III--V compound semiconductors and their alloys," *Journal of Applied Physics,* vol. 89, pp. 5815-5875, 2001.

[9] B. M. Kayes*, et al.*, "Growth of vertically aligned Si wire arrays over large areas (> 1 cm[sup 2]) with Au and Cu catalysts," *Applied Physics Letters,* vol. 91, pp. 103110-3, 2007.

[10] E. I. Givargizov, "Periodic instability in whisker growth," *Journal of Crystal Growth,* vol. 20, p. 217, 1973.

[11] J. F. Geisz*, et al.*, "Lattice-matched GaNPAs-on-silicon tandem solar cells," in *Photovoltaic Specialists Conference, 2005. Conference Record of the Thirty-first IEEE*, 2005, pp. 695-698.

[12] B. M. Kayes*, et al.*, "Comparison of the device physics principles of planar and radial p-n junction nanorod solar cells," *Journal of Applied Physics,* vol. 97, pp. 114302-11, 2005.